Shell Thickness Modulation in Ultrasmall $CdSe/CdS_xSe_{1-x}/CdS$ Core/Shell Quantum Dots *via* 1-Thioglycerol

Anielle Christine A. Silva,[†,*] Sebastião W. da Silva,[‡] Paulo C. Morais,[‡,§] and Noelio O. Dantas[†,*]

[†]Laboratório de Novos Materiais Isolantes e Semicondutores (LNMIS), Institute of Physics, Federal University of Uberlândia, CP 593, Uberlândia MG 38400-902, Brazil, [‡]Center for Applied Physics, Institute of Physics, University of Brasília, Brasília DF 70910-900, Brazil, and [§]School of Automation, Huazhong University of Science and Technology, Wuhan 430074, China

ABSTRACT In this study, we report on the synthesis of CdSe/CdS core—shell ultrasmall quantum dots (CS-USQDs) using an aqueous-based wet chemistry protocol. The proposed chemical route uses increasing concentration of 1-thioglycerol to grow the CdS shell on top of the as-precipitated CdSe core in a controllable way. We found that lower concentration of 1-thioglycerol (3 mmol) added into the reaction medium limits the growth of the CdSe core, and higher and increasing concentration (5—11 mmol) of 1-thioglycerol promotes the growth of CdS shell on top of the CdSe core in a very controllable way, with an increase from 0.50 to 1.25 nm in shell thickness. The growth of CS-USQDs of CdSe/CdS was confirmed by using different experimental techniques, such as optical absorption (OA) spectroscopy, fluorescence spectroscopy, X-ray diffraction, Fourier transform infrared spectroscopy, and Raman spectroscopy. Data collected from OA were used to obtain the average values of the CdSe core diameter, whereas Raman data were used to assess the average values of the CdSe core diameter and CdS shell thicknesses.

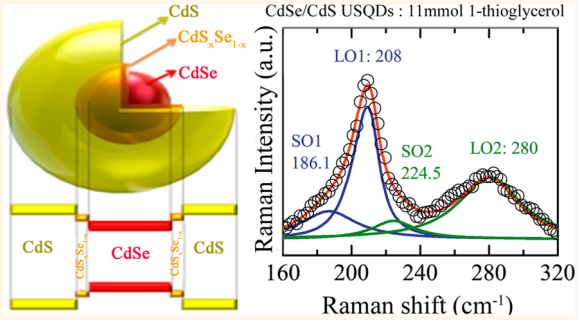

KEYWORDS: CdSe/CdS CS-USQDs · CdSe USQDs · aqueous colloidal solution · 1-thioglycerol concentration

Ultrasmall quantum dots (USQDs) differ from traditional quantum dots (QDs) as they present both much higher fluorescence quantum efficiency and molar absorptivity.[1] Owing to their enhanced physicochemical characteristics, preparation of USQDs has attracted much interest in recent years,[2—4] though few reports regarding reproducible, robust, and costless USQD synthesis routes are found in the literature. Typical synthesis protocols use organometallic precursors[3,4] dispersed in nonaqueous media,[5] in which case and depending on the targeting application require surface manipulation to make the USQDs dispersed in a different end media. However, surface manipulation has its own drawbacks as it may affect both the physicochemical stability and the optical properties of USQDs.[6,7] To avoid surface manipulation while providing a costless and nontoxic preparation protocol, we succeeded in synthesizing MSQDs directly in aqueous medium using a highly reproducible chemical route.[8,9]

Although there are few reports regarding the potential applications for CdSe USQDS, we believed that they can be used as chemical[10—12] and biological sensors[13—15] and solar cells.[16—18] Similarly to traditional QDs, the luminescence of CdSe USQDs can be enhanced using surface-dressing moieties, which reduce incomplete surface bonds and defect levels. Thiol ligands[19—22] are frequently used as surface-coating moieties in aqueous-based protocols as they have strong binding affinity to USQDs' surface in addition to being effective at minimizing differences in surface energies between different facets of growing crystals.[23] Moreover, thiol-based ligands enable USQDs to be isolated while dispersed in aqueous media, thus favoring their use in biotechnology.

Core/shell semiconductor heterostructures have new and interesting optical and optoelectronic properties that can be manipulated using wave function engineering.[24,25] Different optical properties can be engineered depending on the type of semiconductor

* Address correspondence to aniellechristineas@gmail.com, noelio@ufu.br.

Received for review December 18, 2013 and accepted January 25, 2014.

Published online January 27, 2014
10.1021/nn406478f

nanostructure involved and the relative positions of the electron−hole energy levels. Basically, three types of band alignment can be distinguished, namely, type I, type I reverse, and type II.[26] CdSe quantum dots coated with ZnS[27,28] or CdS[29,30] shells are labeled type I band alignment structures. This configuration improves luminescence efficiency and chemical and photochemical stability.[31,32] The reduced lattice mismatch between CdSe and CdS (~3.9%), in comparison to the case of CdSe and ZnS (~12%), facilitates epitaxial growth of the CdS shell around the CdSe core while improving electron accessibility.[32] Core/shell QDs are usually produced using two-step protocols: synthesis and purification of the core first following surface termination with the shell material.[26] The literature reports single-step synthesis approaches for core/shell QDs, as well.[33−35] Recently, Deng *et al.* synthesized CdTe/CdS core/shell MSQDs by varying core−shell composition and shell thickness, thus providing a broad possibility for properties' modulation. Then, light emission can be tuned from visible (480 nm) to near-infrared (820 nm) by overcoating the magic-sized CdTe core with CdS using different shell thicknesses.[21] Silva *et al.* synthesized CdSe/CdS core/shell magic-sized QDs (CS-MSQDs) in aqueous medium and managed to control the CdS shell thickness during the growth process by controlling the synthesis temperature.[33] In the present report, a novel approach to grow CdSe/CdS core/shell ultrasmall quantum dots (CS-USQDs) in aqueous medium in which the CdS shell thickness can be modulated by controlling the 1-thioglycerol concentration is introduced.

RESULTS AND DISCUSSION

Figure 1a shows the optical absorption (OA) and normalized fluorescence (FL) spectra of CdSe-based nanocrystals with increasing concentrations of 1-thioglycerol (*x*T). In all the recorded OA spectra, the lowest energy excitonic band (OA_{exc}) was found at higher energy compared to bulk CdSe (1.74 eV). This finding indicates that all the CdSe-based nanocrystals exhibit quantum confinement effect.[36] In addition, the observed excitonic energy levels were found in the range expected for ultrasmall QDs (USQDs). The CdSe:1T sample shows a wide absorption band, red-shifted with respect to the other CdSe-based samples. This is explained by the relatively lower concentration of the stabilizer (1-thioglycerol) used in the preparation protocol and consequent incomplete surface coating that facilitates rapid nanocrystal growth. The pH 11 of the synthesis protocol is another influencing factor. Several authors[37,38] have observed that higher pH values used in the synthesis protocol favor the growth of larger quantum dots. This is associated with a higher dissociation rate of the precursor compounds[39,40] and lower CdSe solubility,[41−43] which favors QD nucleation and growth. The PL spectra for the CdSe:1T sample show a fluorescence band with a maximum associated with the excitonic transition at approximately 535 nm

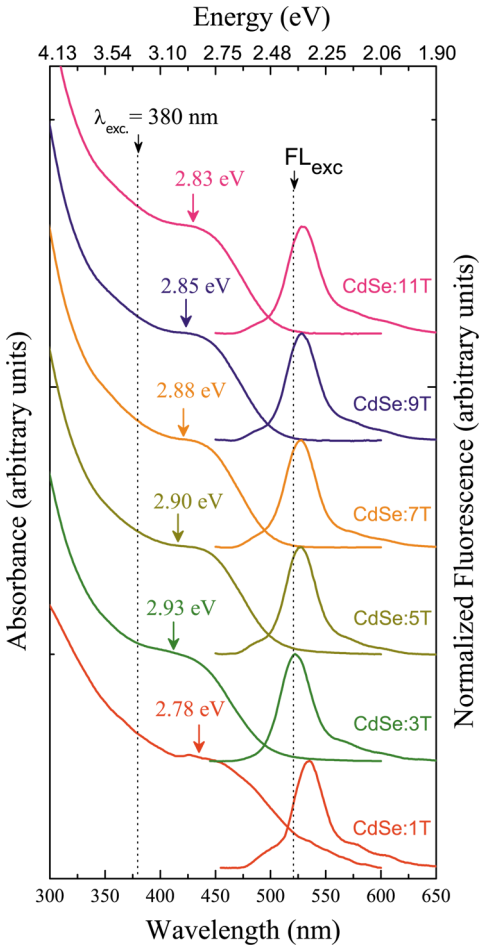

Figure 1. Optical absorption and normalized fluorescence spectra of the CdSe USQDs with increasing concentration (*x*T) of 1-thioglycerol.

(2.31 eV). Two additional features at approximately 577 and 604 nm are attributed to surface defects, which are caused by incomplete passivation of the CdSe USQD surfaces.[44−47] As a result of the higher concentration of 1-thioglycerol used in the synthesis protocol, the exciton OA band of the CdSe:3T sample is blue-shifted with respect to the exciton band of the CdSe:1T sample. Higher concentration of 1-thioglycerol shields the nanocrystal's surface more efficiently, hindering the QD growth and resulting in smaller nanocrystals[48,49] while presenting reduced incomplete surface bonds and defect levels. However, we found a slight red shift in the OA for samples prepared with 1-thioglycerol concentration higher than 3 mmol, which opposes the QD growth limitation caused by the stabilizer.[44,48,50,51]

Actually, the observed red shift provides evidence for the growth of core−shell structures[26] associated with a high degree of mixing in the core and shell LUMOs (molecular orbital model) and a loss of quantum confinement effect (particle-in-a-box model).[32] This evidence of core/shell formation is further supported by the FL spectra (Figure 1). Note that as 1-thioglycerol concentration increases excitonic emission red shifts due

to increased CdS shell thickness, which reduces the quantum confinement effect. In this study, we found that the CdSe quantum dot size is so small that the increase in the stabilizer concentration promotes, besides the coated surface, the onset of the CdS shell. We recently demonstrated that magic-sized QDs (MSQDs) of CdSe/CdS can be synthesized in acid medium, using another method, with a specific concentration of 1-thioglycerol.[33] The average size of the as-produced USQDs was calculated using a well-established empirical equation,[52,53] resulting in 1.9 nm for the CdSe:1T sample and 1.7 nm for sample CdSe:3T.

Figure 2 shows the fluorescence spectra of the as-produced CdSe USQDs with increasing concentration of 1-thioglycerol. The inset shows the fluorescence intensity as a function of 1-thioglycerol concentration. As 1-thioglycerol concentration increases from 1 to 3 mmol, surface shielding improves, reducing incomplete bonds and defect levels, thus intensifying the excitonic fluorescence.[48,49] Furthermore, excitonic emission blue shifts relative to the CdSe:3T sample due to the smaller-sized USQDs, as confirmed by OA spectra (Figure 1). Excitonic emission intensity is higher for samples produced with 5 and 7 mmol of 1-thioglycerol concentration compared to the sample produced with 1 mmol concentration. This increase in the excitonic emission intensity is associated with the formation of a thin CdS shell, which is supported by the slight red shift in the excitonic fluorescence bands of the CdSe:5T and CdSe:7T samples compared with CdSe:3T sample, and red shift of OA bands (see Figure 1).[26] The excitonic fluorescence intensity reaches its highest value at the 7 mmol of 1-thioglycerol concentration, decreasing afterward at higher concentrations of 1-thioglycerol (see inset of Figure 2). The reduction of the luminescence intensity due to the increase of the QD surface stabilizer concentration has already been reported in the literature.[54,55] This trend is claimed to be due to the enhancement of the interaction between the stabilizer molecule and the QD surface, thus increasing the probability of nonradiative electron–hole recombination.[56]

X-ray diffraction patterns of the as-produced CdSe-based USQDs at different 1-thioglycerol concentrations are shown in Figure 3. The recorded patterns were compared with the values found in the standard cards of the following cadmium chalcogenides: (i) CdSe (zinc blende JCPDS no. 19-0191; wurtzite JCPDS no. 77-2307) and (ii) CdS (zinc blende JCPDS no. 42-1411; wurtzite ICSD no. 620319). These observed broad X-ray peaks indicate the extremely small size of the as-produced nanocrystals.[28,57] Furthermore, the as-prepared USQDs present a fraction of mixed phase analysis of the (103) XRD peak, attributed to the CdSe wurtzite structure, confirming that this is the dominant phase.[58,59]

Relative to the CdSe:1T sample, the XRD peaks of the other synthesized samples are slightly shifted to higher

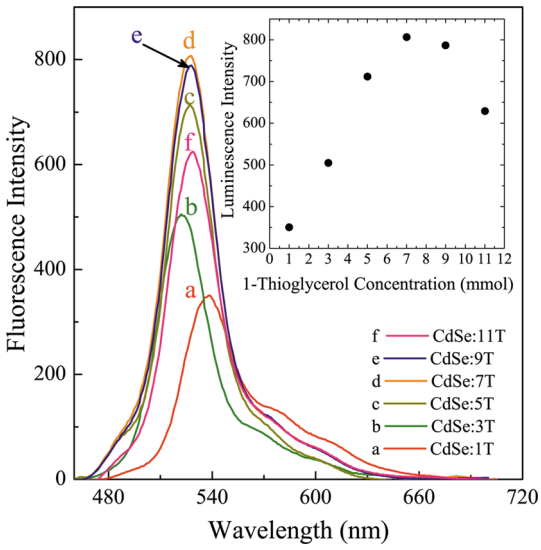

Figure 2. Fluorescence spectra of CdSe USQDs with increasing concentration of 1-thioglycerol. The inset shows fluorescence intensity as a function of 1-thioglycerol concentration.

angle values, toward the angle values of bulk CdS, as the 1-thioglycerol concentration increases. This shift corresponds to the formation of a CdS_xSe_{1-x} alloy or a CdSe/CdS core–shell nanocrystal.[32,34] Furthermore, the formation of the CdS_xSe_{1-x} alloy may cause the blue shift of the OA and FL spectra due to the higher band gap energy of the CdS_xSe_{1-x} alloy compared to the band gap of pure CdSe.[60] This effect is clearly observed in the CdSe:3T sample for which the concentration of 1-thioglycerol used in the synthesis not only shields the surface but also forms the CdS_xSe_{1-x} alloy.[33] The red shifts observed in the OA and FL spectra (Figure 1) in samples CdSe:5T, CdSe:7T, CdSe:9T, and CdSe:11T provide strong evidence of CdSe/CdS core–shell formation. Therefore, the XRD data in combination with the OA and FL data provide strong experimental evidence for the growth of CdS onto the CdSe surface. Moreover, the slight shift of the XRD bands to higher angles confirms that wurtzite CdS is the dominant phase (see Figure 3). This claim is strongly supported by the higher intensity of the hexagonal (101) diffraction peak observed in the CdSe:11T sample, compared to the CdSe:1T sample, and can be attributed to the thicker CdS shell in the CdSe/CdS CS-USQD. The growth and the thickness of the CdS shell are clearly assessed by using Gaussian-like components to fit the XRD band corresponding to the CdSe (100), (002), and (101) peaks for the wurtzite structure, the CdSe (111) peak for the zinc blende structure, the CdS (100), (002), and (101) peaks for the wurtzite structure, and the CdS (111) peak for the zinc blende structure. The fittings provide information regarding the growth and thickness of the CdS shell as the employed concentration of 1-thioglycerol increases, leading to the increase of the intensity of the CdS XRD peak while reducing its fwhm, keeping fixed

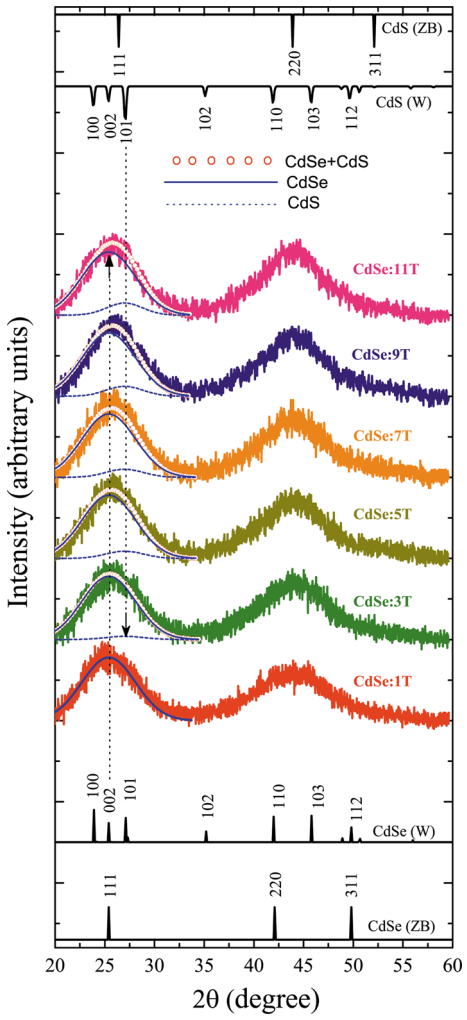

Figure 3. Room temperature XRD patterns of the CdSe USQDs with increasing concentrations of 1-thioglycerol. Standard patterns of the zinc blende and wurtzite phases of CdS (top) and CdSe (bottom) are included for comparison. The fitting of each XRD band around 20−35° is represented by the dotted white/red line (of the CdSe plus CdS patterns), whereas the solid and the dotted blue lines correspond to the CdSe and CdS XRD bands, respectively.

all the parameters describing the CdSe XRD peaks. Furthermore, the observed slight shift of the XRD band toward higher angles confirms that wurtzite CdS is the dominant phase (see arrows in Figure 3). This claim is strongly supported by the higher intensity of the hexagonal (101) diffraction peak observed in the CdSe:11T sample compared with the CdSe:1T sample and can be attributed to the thickest CdS shell found in the as-prepared CdSe/CdS CS-USQDs.[33] Table 1 shows the parameters obtained from the fitting of the XRD data for CdSe and CdS phases, as described above.

The FT-IR spectra of the as-synthesized CdSe-based USQD samples using different concentrations of 1-thioglycerol plus bulk CdS are shown in Figure 4. A broad band in the 3423−3292 cm^{-1} range was observed in the spectra of all CdSe-based samples, which can be associated with OH groups, including adsorption

TABLE 1. Parameters Obtained from the Fitting of the XRD Patterns of As-Produced CdSe USQD Samples with Increasing Concentration of 1-Thioglycerol

	CdSe core			CdS shell		
sample	$x_{0(1)}$ [a]	$\Gamma_{(1)}$ [b]	$A_{(1)}$ [c]	$x_{0(2)}$ [a]	$\Gamma_{(2)}$ [b]	$A_{(2)}$ [c]
CdSe:1T	25.4	2.7	0.78			
CdSe:3T	25.4	2.7	0.78	27	1.98	0.03
CdSe:5T	25.4	2.7	0.78	27	1.92	0.08
CdSe:7T	25.4	2.7	0.78	27	1.89	0.10
CdSe:9T	25.4	2.7	0.78	27	1.86	0.12
CdSe:11T	25.4	2.7	0.78	27	1.80	0.15

[a] Peak positions of the bands. [b] Full width at half-maximum. [c] Band intensities.

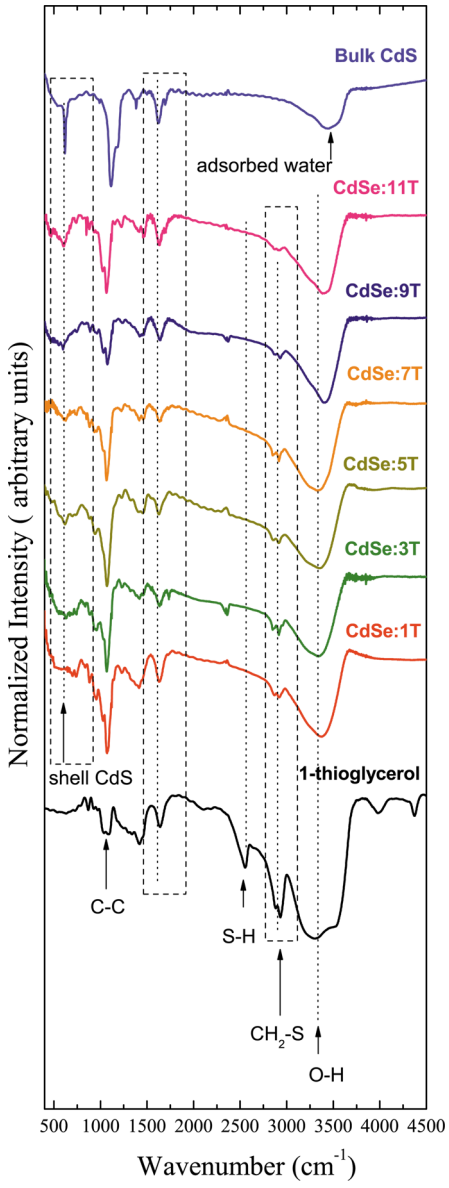

Figure 4. Room temperature FT-IR spectra of 1-thiogycerol, as-produced CdSe USQDs, and bulk CdS.

of water at the surface. However, the shift observed in this band in the CdSe-based USQD samples is due to the

surface-attached OH groups of 1-thioglycerol (Aldrich FT-IR catalog, no. M560-7).[19] Thus, the FT-IR spectra confirm that the OH functional groups remain intact on the surface of the USQD samples. Pure 1-thioglycerol FT-IR spectrum (see Figure 4) shows peaks at 867 and 2600 cm^{-1}, which correspond, respectively, to the bending and stretching modes of the S−H bonding.[61] Additionally, 1-thioglycerol FT-IR spectrum presents a feature at 2850 cm^{-1}, corresponding to the CH_2−S bonding.[62,63] However, in the FT-IR spectra of the as-produced USQD samples, we found no peak at 2600 cm^{-1}, corresponding to the S−H stretching mode. Additionally, in as-produced CdSe-based USQD samples, we found a strong reduction of the IR feature peaking at 2914 cm^{-1} (CH_2−S bonding). These findings support the onset of covalent bonds between S (from 1-thioglycerol thiol groups) and Cd^{2+} ions at the QD surface, thus building the CdS shell onto the CdSe USQD's surface. This picture is in very good agreement with the results obtained from OA, FL, and XRD, showing that the growth of CdS shell onto an extremely small CdSe core can be controlled *via* modulation of the 1-thioglycerol concentration in order to produce CdSe/CdS CS-USQDs.

In order to provide further evidence of the formation and growth of the CdS shell onto the CdSe core while increasing the 1-thioglycerol concentration, we used Raman spectroscopy. The Raman spectra of the CdSe USQD samples produced while increasing the 1-thioglycerol concentration are shown in Figure 5. In order to describe the Raman spectra and to calculate the size of the CdSe core and CdS shell thickness, we used our modified phonon confinement model.[33] The data presented in Figure 5 display an excellent agreement between the experimental data (open symbols) and the fitting curves (red solid lines).[33] Figure 5a,b shows the Raman spectra of samples CdSe:1T and CdSe:3T, respectively, in which the CdSe Raman-active longitudinal optical (LO) (ω_{LO1}) and surface optical (SO) (ω_{SO1}) vibrational modes are observed. The intensity $I(\omega)$ related to the experimental Raman spectrum was fitted, $I(\omega) = I^{(1)}_{LO}(\omega) + I^{(1)}_{SO}(\omega)$. The first-order LO Raman ($I^{(1)}_{LO}(\omega)$) spectrum is then obtained by the following expression:[64,65]

$$I^{(i)}_{LO}(\omega) \approx \int \frac{d^3q|C_{(i)}(0,\boldsymbol{q})|^2}{[\omega - \omega_{(i)}(\boldsymbol{q})]^2 + (\Gamma_{(i)}/2)^2} \qquad (2)$$

where the Fourier coefficients for the Gaussian function are given by $|C_{(i)}(0,q)|^2 \approx \exp(-q^2_{(i)}\sigma^2_{(i)})$, $d^3q \approx q^2\,dq$ due to the nanocrystals' spherical symmetry, and here the *i* number (1) represents CdSe. The values of LO phonon frequency ($\omega_{0(1)}$) at the Γ-point ($q = 0$) and the natural line width (fwhm) of the zone center optical phonon (Γ_{LO1}) describe the average phonon dispersion in the CdSe, $\omega_{(1)}(q) = \omega_{0(1)} - \Delta\omega_{(1)}q^2_{(1)}$; here there is formation of interfacial alloying. The wave-vector $q_{(1)}$ is represented in units of $2\pi/_{(1)}$, that is, $q_{(i)} \equiv [q_{(i)}/(2\pi/)]$,

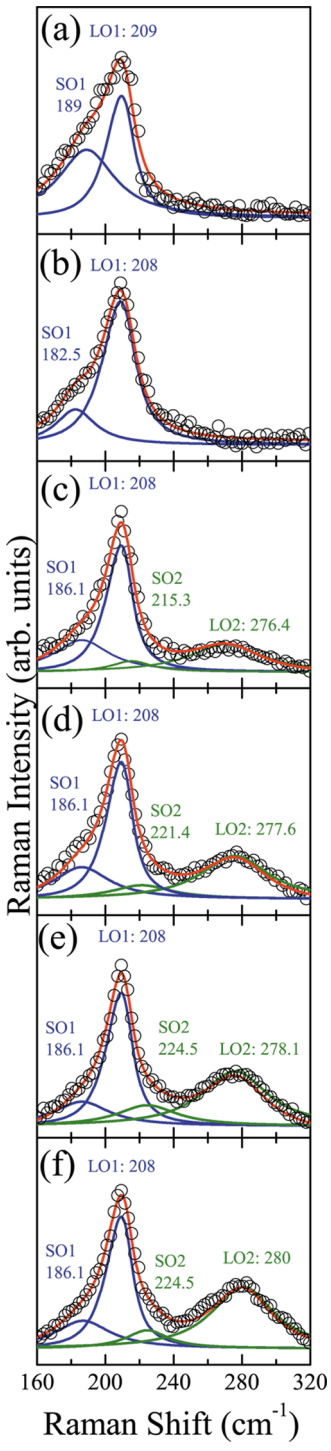

Figure 5. Room temperature Raman spectra (open symbols) of CdSe USQDs synthesized with increasing concentration of 1-thioglycerol: (a) CdSe:1T; (b) CdSe:3T; (c) CdSe:5T; (d) CdSe:7T; (e) CdSe:9T; (f) CdSe:11T. The frequency of each vibrational mode (SO1, LO1, SO2, or LO2) is indicated by numbers. The fitting of each Raman spectrum is represented by the red solid line, with subspectrum represented by a blue solid line for vibrations related to the core and green solid line for vibrations related to the shell.

with a mean lattice parameter of the wurtzite structure given by Singha *et al.*[58] Since the average phonon dispersion is described by a nonperiodic function, we

TABLE 2. Parameters (in units of cm^{-1}) Obtained from the Fitting of the Raman Spectra of As-Produced CdSe USQD Samples with Increasing Concentration of 1-Thioglycerol

	CdSe core						CdS shell					
sample	$\omega_{0(1)}$[a]	$\Delta\omega_{(1)}$	ω_{LO1}	Γ_{LO1}[b]	ω_{SO1}	Γ_{SO1}	$\omega_{0(2)}$[a]	$\Delta\omega_{(2)}$	ω_{LO2}	Γ_{LO2}[b]	ω_{SO2}	Γ_{SO2}
CdSe:1T	214	69	209	15	189	20						
CdSe:3T	214	60	208	18	182.5	14.1						
CdSe:5T	214	60	208	18	186.1	19.5	282	60	276.4	47.5	215.3	17.9
CdSe:7T	214	60	208	18	186.1	19.5	282	60	277.6	44	221.4	21.3
CdSe:9T	214	60	208	18	186.1	19.5	282	60	278.1	43	224.5	20.7
CdSe:11T	214	60	208	18	186.1	19.5	282	60	280	40	224.7	19.5

[a] LO phonon frequency at the Γ-point ($q = 0$). [b] Γ_{L01} and Γ_{L02} are the fwhm for CdSe and CdS, respectively.

have carried out the integration in the first Brillouin zone.

The SO mode is described as follows:[58,66]

$$I_{SO}^{(i)}(\omega) = \frac{B_{(i)}\Gamma_{SO(i)}}{(\omega - \omega_{SO(i)})^2 + \Gamma_{SO(i)}^2} \quad (3)$$

where $\Gamma_{SO(i)}$ and $\omega_{SO(i)}$ are, respectively, the fwhm and the SO phonon frequency and $B_{(i)}$ is an arbitrary constant.

In Figure 5a, note that the high-frequency shoulder expected from spherical nanocrystals[65,67,68] was not observed, thus providing evidence that the protocol we used to produce the CdSe:1T sample allowed partial elimination of surface bonds/defects with the CdS_xSe_{1-x} alloy formation around the CdSe USQD core. The confirmation of the CdS_xSe_{1-x} alloying while using 1-thioglycerol at 1 mmol is supported by the change of the bandwidth value related to the LO branch with respect to bulk CdSe ($\Delta\omega = 118$ cm^{-1}) (see Table 2).[33] In Figure 5b (CdSe:3T sample), both the CdSe LO and the SO vibrational modes are shifted to lower frequencies compared to the CdSe:1T sample (see Figure 5a). This finding gives evidence that the average size of the USQD CdSe core in sample CdSe:3T is smaller than that in sample CdSe:1T. This result was also confirmed from the OA and FL data (Figure 1) plus the calculation of the CdSe USQD core size using our modified phonon confinement model described in the literature (see Table 3).[33]

Figure 5c−f shows the Raman spectra of the CdSe/CdS CS-USQDs. Besides the Raman peak position (ω_{LO1}) at ≈208 cm^{-1}, an additional Raman peak (ω_{LO2}) appears at ≈276.4 cm^{-1} for sample CdSe:5T (Figure 5c), at ≈277.6 cm^{-1} for sample CdSe:7T (Figure 5d), at ≈278.1 cm^{-1} for sample CdSe:9T (Figure 5e), and at ≈280 cm^{-1} for sample CdSe:11T (Figure 5f), confirming the CdS shell growth onto the CdSe USQD core. To describe these Raman spectra, the intensity $I(\omega)$ related to the experimental Raman spectrum was fitted, $I(\omega) = I_{LO}^{(1)}(\omega) + I_{SO}^{(1)}(\omega) + I_{LO}^{(2)}(\omega) + I_{SO}^{(2)}(\omega)$. In this case, we have defined the integer values as $i = 1$ for vibrations around the confined modes of the CdSe core and $i = 2$ for vibrations around the modes of the CdS shell. The Fourier coefficient used to calculate the $I_{LO}^{(i)}(\omega)$ intensity regarding

TABLE 3. Mean Dimensions (all in nm) of Core CdSe USQDs and CdS Shell Thickness Evaluated by the Raman and OA Results

	CdSe core size		CdS shell thickness
sample	Raman	OA	Raman
CdSe:1T	1.81	1.90	
CdSe:3T	1.59	1.70	
CdSe:5T	1.59		0.50
CdSe:7T	1.59		0.83
CdSe:9T	1.59		1.04
CdSe:11T	1.59		1.25

confined LO phonons was given by $|C_{(1)}(0,q)|^2 \approx \exp(-q_{(1)}^2\sigma_{(1)}^2)$ and $|C_{(j)}(0,q)|^2 \approx \{2\pi\sigma_{(j)}^2[\sigma_{(j)}^2 + r_{(j)}^2]^2 - 2\sigma_{(j)}^2q^2 + 2\sigma_{(j)}^4r_{(j)}^2q^2 + \sigma_{(j)}^8q^4\}\exp(-\sigma_{(j)}^2q^2)$ to CdSe core and CdS shell, respectively.[33] Furthermore, the parameters $r_{(j=m)} = [(d + \sum_{k=1}^{m} t_{(k)})/2]$, where k is an integer number associated with every internal shell and normalized σ parameter of the Gaussian function proposed by Silva *et al.*[33] Mean lattice parameter of wurtzite structure is given by[58] $\bar{a}_{(1)} = 0.608$ nm for the CdSe and $\bar{a}_{(2)} = 0.582$ nm for the CdS.

It is worth noting, in Figure 5c−f, that we found the ω_{LO1} phonon frequency associated with the CdSe core unchanged while growing the CdS shell on top of it, demonstrating that any possible strain effect involving the core−shell interface can be neglected. This is justified by the presence of the wurtzite phase, as the lattice mismatch between the CdSe core and the CdS shell is too small to be detected through Raman measurements.[58,66] According to this finding, we can confirm a contribution of the wurtzite phase in the XRD data (Figure 3). Thus, in Table 2, the observed blue shift of the ω_{LO2} frequency is due to the weakening of the LO phonon confinement in the shell, which is caused by the increase of the CdS shell thickness (as shown in Table 3). This result supports the picture from which the increase of the 1-thioglycerol concentration (over 5 mmol) promotes the formation and growth of the CdS shell. No changes were observed in other parameters, such as the $\omega_{0(1)}$ and Γ_{LO1} of the core and the shell parameters ($\omega_{0(2)}$ and $\Delta\omega_{(2)}$), related to the CdS_xSe_{1-x}

interfacial alloy. In a recent publication, we reported on the synthesis of CdSe/CdS CS-MSQDs[33] and verified that the effects of the alloy are much stronger than in the present study. Thus, on the basis of our findings, we can say that the increase of the size of the quantum dots decreases the influence of the interfacial alloy on the core and shell phonon dispersions. Another interesting feature is that the basic pH medium employed during the synthesis process herein described favored the surface anchoring of the 1-thioglycerol (providing an alloy at 1 mmol), and as one increases the stabilizer concentration, a more homogeneous CdS shell (evidenced by the decrease in Γ_{LO2}) is obtained. The reduction of the ω_{SO1} phonon frequency from the CdSe:1T sample to the CdSe:3T sample is due to the reduction of the NC size. Actually, the increase of the NC size leads to a blue shift of both the LO and the SO Raman modes due to the reduction of the quantum confinement.[65] However, the increase of the ω_{SO1} frequency from the CdSe:3T sample to the CdSe:5T sample is due to the influence of the complex molecular structure of the stabilizing ligand, and the variety of surface configurations in the adsorbed state on the surface phonon of the bare CdSe USQDs can be more complicated than simply an effective dielectric constant.[69] Finally, the blue shift of the ω_{SO2} phonon frequency is explained within the dielectric continuum approach.[68] Thus, in the present study, we provided evidence that supports the controlled growth of the CdS shell onto the CdSe USQD core using a new methodology. The controlled growth of the CdS shell can also be achieved by modulating the temperature of the synthesis, as recently reported.[33]

The calculated mean values associated with the core diameters and the shell thicknesses are shown in Table 3. The calculated values (1.81 nm (CdSe:1T) and 1.59 nm (CdSe:3T until CdSe:11T)) presented in Table 3 were obtained from the fitting procedures using our modified phonon confinement model[33] employed in the analysis of the Raman spectra of the USQD CdSe samples with increasing 1-thioglycerol concentration. These values are associated with normalized σ parameter, beginning with $\sigma = d/\sqrt{20}$ for core (d = CdSe core size) and $\sigma = t/\sqrt{20}$ for shell (t = CdS shell thicknesses).[33] Additionally, we compared these calculated values with those obtained from the core size estimation using the empirical equation to analyze the OA spectra. The mean diameters obtained from the AO spectra agree quite well with the values obtained from the fitting procedure of the Raman spectra using the modified phonon confinement mode.[33] The slight differences observed between the two aforementioned calculating approaches can be attributed to the uncertainty of the maximum of the OA band due to the relatively broad line width.

CONCLUSIONS

In this study, we report on an aqueous-based chemical synthesis protocol that successfully grew ultrasmall quantum dots of CdSe surface dressed with a CdS shell layer of controllable thicknesses. We found that lower concentration of 1-thioglycerol (3 mmol) added into the reaction medium limits the growth of the CdSe core, whereas higher and increasing concentration (5−11 mmol) of 1-thioglycerol promotes the growth of the CdS shell on top of the CdSe core in a very controllable way, ranging from 0.5 nm to 1.25 nm in shell thickness. The growth of core−shell ultrasmall quantum dots of CdSe/CdS was confirmed by using different experimental techniques, such as optical absorption spectroscopy, fluorescence spectroscopy, X-ray diffraction (XRD), Fourier transform infrared (FT-IR) spectroscopy, and Raman spectroscopy (RS). As the 1-thioglycerol concentration increases, the red shift of the excitonic absorption bands confirms the growth of the CdS shell layer with increasing thickness, whereas the XRD patterns of the CS-USQDs show the growth of USQD CdSe core with the typical XRD features shifted to higher angles. These findings provide strong evidence of the CdSe/CdS CS-USQD formation. The FT-IR spectra show characteristic CdS absorptions demonstrating that the sulfur provided by 1-thioglycerol covalently bonds with cadmium ions at the surface of the CdSe USQDs to build the CdS shell. Furthermore, the Raman data confirmed the growth of the CdS shell with increasing thickness as the 1-thioglycerol concentration increases. The average diameter of the ultrasmall CdSe core as well as the average thickeness of the CdS shell was calculated using our modified phonon confinement model. The synthesis protocol herein introduced, based on the addition of 1-thioglycerol into the reaction medium at increasing concentration, not only gives control over the CdSe core size but also provides fine control of the CdSe shell thickness while growing CdSe/CdS CS-USQDs. The methodology presented in this report, which is highly reproducible and inexpensive, is expected to be useful for producing CS-USQDs of different II−IV-based semiconductor materials. Furthermore, the hydroxyl groups facing outward on the CS-USQDs allow the as-grown nanostructures to be easily dispersed in aqueous media, incorporating into them promising biotechnological applications.

EXPERIMENTAL SECTION

Materials. Selenium powder (Se, 99.999%), sodium borohydride ($NaBH_4$, 98%), cadmium perchlorate hexahydrate ($Cd(ClO_4)_2 \cdot 6H_2O$, 99.999%), sodium hydroxide (NaOH), and 1-thioglycerol (>97%) were all purchased from Sigma-Aldrich (Brazil) and used without further purification. Ultrapure water used in the preparation of aqueous solutions was obtained from the QUIMIS system.

Synthesis of CdSe and CdSe/CdS Ultrasmall Quantum Dots. CdSe USQDs and CdSe/CdS CS-USQDs were grown in aqueous solutions at room temperature using the following steps. Selenium powder (mmol) and $NaBH_4$ (mmol) were dispersed in ultrapure water (20 mL) in a three-neck flask under argon flow. Next, 2 mmol of $Cd(ClO_4)_2 \cdot 6H_2O$ and *x* mmol of 1-thioglycerol (*x*T) were mixed in ultrapure water, and the pH was adjusted to 11 by adding 0.1 M NaOH. The concentrations (*x*) of 1-thioglycerol employed were 1, 3, 5, 7, 9, and 11 mmol. Cadmium- (*x*T) and selenium-containing solutions were mixed under magnetic stirring in a three-neck flask under argon flow at room temperature for 30 min. The resulting suspensions containing CdSe USQDs and CdSe/CdS CS-USQDs were labeled CdSe:1T, CdSe:3T, CdSe:5T, CdSe:7T, CdSe:9T, and CdSe:11T. CdSe USQDs and CdSe/CdS CS-USQDs were precipitated with ethanol and centrifuged four times at 6000 rpm for 10 min. The resulting nanopowders were dried in vacuum (mechanical pump) at room temperature and further dispersed in ultrapure water at a concentration of 1.4 mg/mL.

Characterization. Optical absorption spectra were recorded at room temperature using a double-beam UV−vis−NIR spectrophotometer (Shimadzu UV-3600), operating between 300 and 600 nm, at a spectral resolution of 1 nm. The quantum dot solutions were diluted (0.035 mg/mL) using ultrapure water for OA measurements. Fluorescence spectra were recorded with a Cary Eclipse spectrophotometer (Varian) using the 380 nm wavelength from a xenon lamp as the excitation source, with a concentration of 1.4 mg/mL. Room temperature X-ray diffraction patterns of the nanopowders were recorded with a XRD-6000 Shimadzu diffractometer. Monochromatic Cu $K\alpha_1$ radiation (λ = 1.54056 Å) was used to identify the structural phase of the as-produced samples. The infrared (IR) spectra of the samples were recorded at room temperature using a Shimadzu FT-IR spectrophotometer (IR Prestige-21) in transmission mode, operating in the spectral range from 450 to 4600 cm^{-1} at a resolution of 4 cm^{-1}. A pure KBr disk was first pressed, and its IR spectrum was measured and determined to be IR-transparent. Then, KBr was mixed with the as-produced nanopowders and pressed in a disk-shaped probing sample for IR measurements. Room temperature Stokes Raman scattering spectra of the as-precipitated powders were recorded with a JY-T64000 micro-Raman spectrometer excited with the low-power Ar^+ 514 nm laser line and detected in backscattering geometry. It used an objective of 50× to focus the laser beam down to a spot of 1.5 μm in diameter. Thus, the laser power and the power density hitting the sample were 5 mW and 3×10^5 W/cm^2, respectively. Therefore, any heating effect on the vibrational spectra of the samples was neglected.

Conflict of Interest: The authors declare no competing financial interest.

Acknowledgment. The authors gratefully acknowledge financial support from the CAPES, FAPEMIG, MCT/CNPq, and NANOBIOTEC Brazil. We are also grateful for use of the Cary Eclipse spectrophotometer (Varian) supported by NANOBIOTEC Brazil, XRD-6000 Shimadzu diffractometer at the Institute of Chemistry, Federal University of Uberlândia (UFU), and supported by the grant "Pró-Equipamentos" from the Brazilian Agency CAPES, and FT-IR spectrophotometer (model IR Prestige-21) of the Shimadzu supported by Shimadzu Brazil.

REFERENCES AND NOTES

1. Beri, R. K.; Khanna, P. K.; Singh, V.; Mehta, B. R. "Yellow Emitting" Magic-Size Cadmium Selenide Nanocrystals *via* a Simplified Spray Pyrolysis Method. *Curr. Appl. Phys.* **2011**, *11*, 809–811.
2. Yoon, J. H.; Chae, W. S.; Im, S. J.; Kim, Y. R. Mild Synthesis of Ultra-small CdSe Quantum Dots in Ethylenediamine Solution. *Mater. Lett.* **2005**, *59*, 1430–1433.
3. Ahamefula, U. C.; Sulaiman, M. Y.; Ibarahim, Z.; Ibrahim, N. B.; Othman, M. Y. Low-Temperature Synthesis and Characterisation of Ultra-small Cadmium Selenide Quantum Dots in Octadecene Solution. *Energy Procedia* **2012**, *25*, 62–69.
4. Ma, W. L.; Swisher, S. L.; Ewers, T.; Engel, J.; Ferry, V. E.; Atwater, H. A.; Alivisatos, A. P. Photovoltaic Performance of Ultrasmall PbSe Quantum Dots. *ACS Nano* **2011**, *5*, 8140–8147.
5. Zhan, H. J.; Zhou, P. J.; Pan, K. L.; He, T.; He, X.; Zhou, C. Y.; He, Y. N. One-Pot Aqueous-Phase Synthesis of Ultra-small CdSe/CdS/CdZnS Core−Shell−Shell Quantum Dots with High-Luminescent Efficiency and Good Stability. *J. Nanopart. Res.* **2013**, *15*, 1680.
6. Chen, X. B.; Samia, A. C. S.; Lou, Y. B.; Burda, C. Investigation of the Crystallization Process in 2 nm CdSe Quantum Dots. *J. Am. Chem. Soc.* **2005**, *127*, 4372–4375.
7. Xia, Y.-S.; Zhu, C.-Q. Aqueous Synthesis of Luminescent Magic Sized CdSe Nanoclusters. *Mater. Lett.* **2008**, *62*, 2103–2105.
8. Baker, J. S.; Nevins, J. S.; Coughlin, K. M.; Colón, L. A.; Watson, D. F. Influence of Complex-Formation Equilibria on the Temporal Persistence of Cysteinate-Functionalized CdSe Nanocrystals in Water. *Chem. Mater.* **2011**, *23*, 3546–3555.
9. Soloviev, V. N.; Eichhofer, A.; Fenske, D.; Banin, U. Molecular Limit of a Bulk Semiconductor: Size Dependence of the "Band Gap" in CdSe Cluster Molecules. *J. Am. Chem. Soc.* **2000**, *122*, 2673–2674.
10. Mandal, A.; Dandapat, A.; De, G. Magic Sized ZnS Quantum Dots as a Highly Sensitive and Selective Fluorescence Sensor Probe for Ag^+ Ions. *Analyst* **2012**, *137*, 765–772.
11. Frasco, M. F.; Chaniotakis, N. Semiconductor Quantum Dots in Chemical Sensors and Biosensors. *Sensors* **2009**, *9*, 7266–7286.
12. Dong, Y.; Wang, R.; Li, G.; Chen, C.; Chi, Y.; Chen, G. Polyamine-Functionalized Carbon Quantum Dots as Fluorescent Probes for Selective and Sensitive Detection of Copper Ions. *Anal. Chem.* **2012**, *84*, 6220–6224.
13. Maestro, L. M.; Rodriguez, E. M.; Rodriguez, F. S.; la Cruz, M. C.; Juarranz, A.; Naccache, R.; Vetrone, F.; Jaque, D.; Capobianco, J. A.; Sole, J. G. CdSe Quantum Dots for Two-Photon Fluorescence Thermal Imaging. *Nano Lett.* **2010**, *10*, 5109–5115.
14. Khalil, W. K.; Girgis, E.; Emam, A. N.; Mohamed, M. B.; Rao, K. V. Genotoxicity Evaluation of Nanomaterials: DNA Damage, Micronuclei, and 8-Hydroxy-2-deoxyguanosine Induced by Magnetic Doped CdSe Quantum Dots in Male Mice. *Chem. Res. Toxicol.* **2011**, *24*, 640–650.
15. Bednarkiewicz, A.; Nyk, M.; Samoc, M.; Strek, W. Up-conversion FRET from Er^{3+}/Yb^{3+}:$NaYF_4$ Nanophosphor to CdSe Quantum Dots. *J. Phys. Chem. C* **2010**, *114*, 17535–17541.
16. Chen, Z.; Zhang, H.; Xing, Z.; Hou, J.; Li, J.; Wei, H.; Tian, W.; Yang, B. Aqueous-Solution-Processed Hybrid Solar Cells with Good Thermal and Morphological Stability. *Sol. Energy Mater. Sol. Cells* **2013**, *109*, 254–261.
17. Chen, Z.; Zhang, H.; Du, X.; Cheng, X.; Chen, X.; Jiang, Y.; Yang, B. From Planar-Heterojunction to n−i Structure: An Efficient Strategy To Improve Short-Circuit Current and Power Conversion Efficiency of Aqueous-Solution-Processed Hybrid Solar Cells. *Energy Environ. Sci.* **2013**, *6*, 1597.
18. Chen, Z.; Zhang, H.; Yu, W.; Li, Z.; Hou, J.; Wei, H.; Yang, B. Inverted Hybrid Solar Cells from Aqueous Materials with a PCE of 3.61%. *Adv. Energy Mater.* **2013**, *3*, 433–443.
19. Artemyev, M. V.; Woggon, U.; Jaschinski, H.; Gurinovich, L. I.; Gaponenko, S. V. Spectroscopic Study of Electronic States in an Ensemble of Close-Packed CdSe Nanocrystals. *J. Phys. Chem. B* **2000**, *104*, 11617–11621.
20. Gaponik, N.; Talapin, D. V.; Rogach, A. L.; Hoppe, K.; Shevchenko, E. V.; Kornowski, A.; Eychmuller, A.; Weller, H. Thiol-Capping of CdTe Nanocrystals: An Alternative to Organometallic Synthetic Routes. *J. Phys. Chem. B* **2002**, *106*, 7177–7185.
21. Deng, Z. T.; Schulz, O.; Lin, S.; Ding, B. Q.; Liu, X. W.; Wei, X. X.; Ros, R.; Yan, H.; Liu, Y. Aqueous Synthesis of Zinc Blende CdTe/CdS Magic-Core/Thick-Shell Tetrahedral-Shaped Nanocrystals with Emission Tunable to Near-Infrared. *J. Am. Chem. Soc.* **2010**, *132*, 5592.
22. Vinayaka, A. C.; Thakur, M. S. Photoabsorption and Resonance Energy Transfer Phenomenon in CdTe−Protein Bioconjugates: An Insight into QD−Biomolecular Interactions. *Bioconjugate Chem.* **2011**, *22*, 968–75.

23. Zhang, H.; Wang, D.; Yang, B.; Mohwald, H. Manipulation of Aqueous Growth of CdTe Nanocrystals To Fabricate Colloidally Stable One-Dimensional Nanostructures. *J. Am. Chem. Soc.* **2006**, *128*, 10171–10180.
24. Talapin, D. V.; Lee, J. S.; Kovalenko, M. V.; Shevchenko, E. V. Prospects of Colloidal Nanocrystals for Electronic and Optoelectronic Applications. *Chem. Rev.* **2010**, *110*, 389–458.
25. Zipper, E.; Kurpas, M.; Maśka, M. M. Wave Function Engineering in Quantum Dot–Ring Nanostructures. *New J. Phys.* **2012**, *14*, 093029.
26. Reiss, P.; Protiere, M.; Li, L. Core/Shell Semiconductor Nanocrystals. *Small* **2009**, *5*, 154–168.
27. Dabbousi, B. O.; RodriguezViejo, J.; Mikulec, F. V.; Heine, J. R.; Mattoussi, H.; Ober, R.; Jensen, K. F.; Bawendi, M. G. (CdSe)ZnS Core–Shell Quantum Dots: Synthesis and Characterization of a Size Series of Highly Luminescent Nanocrystallites. *J. Phys. Chem. B* **1997**, *101*, 9463–9475.
28. Talapin, D. V.; Rogach, A. L.; Kornowski, A.; Haase, M.; Weller, H. Highly Luminescent Monodisperse CdSe and CdSe/ZnS Nanocrystals Synthesized in a Hexadecylamine–Trioctylphosphine Oxide–Trioctylphospine Mixture. *Nano Lett.* **2001**, *1*, 207–211.
29. Greytak, A. B.; Allen, P. M.; Liu, W.; Zhao, J.; Young, E. R.; Popović, Z.; Walker, B. J.; Nocera, D. G.; Bawendi, M. G. Alternating Layer Addition Approach to CdSe/CdS Core/Shell Quantum Dots with Near-Unity Quantum Yield and High On-Time Fractions. *Chem. Sci.* **2012**, *3*, 2028.
30. Talapin, D. V.; Nelson, J. H.; Shevchenko, E. V.; Aloni, S.; Sadtler, B.; Alivisatos, A. P. Seeded Growth of Highly Luminescent CdSe/CdS Nanoheterostructures with Rod and Tetrapod Morphologies. *Nano Lett.* **2007**, *7*, 2951–2959.
31. Hines, M. A.; Guyot-Sionnest, P. Synthesis and Characterization of Strongly Luminescing ZnS-Capped CdSe Nanocrystals. *J. Phys. Chem.* **1996**, *100*, 468–471.
32. Peng, X. G.; Schlamp, M. C.; Kadavanich, A. V.; Alivisatos, A. P. Epitaxial Growth of Highly Luminescent Cdse/Cds Core/Shell Nanocrystals with Photostability and Electronic Accessibility. *J. Am. Chem. Soc.* **1997**, *119*, 7019–7029.
33. Silva, A. C. A.; Neto, E. S. F.; da Silva, S. W.; Morais, P. C.; Dantas, N. O. Modified Phonon Confinement Model and Its Application to CdSe/CdS Core–Shell Magic-Sized Quantum Dots Synthesized in Aqueous Solution by a New Route. *J. Phys. Chem. C* **2013**, *117*, 1904–1914.
34. Mekis, I.; Talapin, D. V.; Kornowski, A.; Haase, M.; Weller, H. One-Pot Synthesis of Highly Luminescent CdSe/CdS Core–Shell Nanocrystals *via* Organometallic and "Greener" Chemical Approaches. *J. Phys. Chem. B* **2003**, *107*, 7454–7462.
35. Xie, R.; Zhong, X.; Basché, T. Synthesis, Characterization, and Spectroscopy of Type-II Core/Shell Semiconductor Nanocrystals with ZnTe Cores. *Adv. Mater.* **2005**, *17*, 2741–2745.
36. Neeleshwar, S.; Chen, C.; Tsai, C.; Chen, Y.; Shyu, S.; Seehra, M. Size-Dependent Properties of CdSe Quantum Dots. *Phys. Rev. B* **2005**, *71*, 201307(R).
37. Etxeberria, H.; Kortaberria, G.; Zalakain, I.; Larrañaga, A.; Mondragon, I. Effect of Different Aqueous Synthesis Parameters on the Size of CdSe Nanocrystals. *J. Mater. Sci.* **2012**, *47*, 7167–7174.
38. Rogach, A. L.; Kornowski, A.; Gao, M. Y.; Eychmuller, A.; Weller, H. Synthesis and Characterization of a Size Series of Extremely Small Thiol-Stabilized CdSe Nanocrystals. *J. Phys. Chem. B* **1999**, *103*, 3065–3069.
39. Uchil, J.; Pattabi, M. Effect of pH on the Size of CdS Nanoparticles Synthesized by Chemical Diffusion Across a Biological Membrane. *J. New Mater. Electrochem. Syst.* **2005**, *8*, 155–161.
40. Singh, S.; Garg, S.; Chahal, J.; Raheja, K.; Singh, D.; Singla, M. L. Luminescent Behavior of Cadmium Sulfide Quantum Dots for Gallic Acid Estimation. *Nanotechnology* **2013**, *24*, 115602.
41. Siy, J. T.; Bartl, M. H. Insights into Reversible Dissolution of Colloidal CdSe Nanocrystal Quantum Dots. *Chem. Mater.* **2010**, *22*, 5973–5982.
42. Aldana, J.; Wang, Y. A.; Peng, X. G. Photochemical Instability of CdSe Nanocrystals Coated by Hydrophilic Thiols. *J. Am. Chem. Soc.* **2001**, *123*, 8844–8850.
43. Mahmoud, W. E.; Yaghmour, S. J. Synthesis, Characterization and Luminescence Properties of Thiol-Capped CdSe Quantum Dots at Different Processing Conditions. *Opt. Mater.* **2013**, *35*, 652–656.
44. Wuister, S. F.; Donega, C. D.; Meijerink, A. Influence of Thiol Capping on the Exciton Luminescence and Decay Kinetics of CdTe and CdSe Quantum Dots. *J. Phys. Chem. B* **2004**, *108*, 17393–17397.
45. Babentsov, V.; Sizov, F. Defects in Quantum Dots of IIB–VI Semiconductors. *Opto-Electron. Rev.* **2008**, *16*, 208–225.
46. Kortan, A. R.; Hull, R.; Opila, R. L.; Bawendi, M. G.; Steigerwald, M. L.; Carroll, P. J.; Brus, L. E. Nucleation and Growth of Cdse on ZnS Quantum Crystallite Seeds, and Vice Versa, in Inverse Micelle Media. *J. Am. Chem. Soc.* **1990**, *112*, 1327–1332.
47. Park, Y. S.; Dmytruk, A.; Dmitruk, I.; Kasuya, A.; Okamoto, Y.; Kaji, N.; Tokeshi, M.; Baba, Y. Aqueous Phase Synthesized CdSe Nanoparticles with Well-Defined Numbers of Constituent Atoms. *J. Phys. Chem. C* **2010**, *114*, 18834–18840.
48. Pal, M.; Mathews, N. R.; Santiago, P.; Mathew, X. A Facile One-Pot Synthesis of Highly Luminescent CdS Nanoparticles Using Thioglycerol as Capping Agent. *J. Nanopart. Res.* **2012**, *14*, 916.
49. Wuister, S. F.; Meijerink, A. Synthesis and Luminescence of CdS Quantum Dots Capped with a Silica Precursor. *J. Lumin.* **2003**, *105*, 35–43.
50. Sondi, I.; Siiman, O.; Matijevic, E. Synthesis of CdSe Nanoparticles in the Presence of Aminodextran as Stabilizing and Capping Agent. *J. Colloid Interface Sci.* **2004**, *275*, 503–507.
51. Unni, C.; Philip, D.; Gopchandran, K. G. Studies on Optical Absorption and Photoluminescence of Thioglycerol-Stabilized CdS Quantum Dots. *Spectrochim. Acta, Part A* **2008**, *71*, 1402–7.
52. Yu, W. W.; Qu, L. H.; Guo, W. Z.; Peng, X. G. Experimental Determination of the Extinction Coefficient of CdTe, CdSe, and CdS Nanocrystals. *Chem. Mater.* **2003**, *15*, 2854–2860.
53. Riehle, F. S.; Bienert, R.; Thomann, R.; Urban, G. A.; Krugert, M. Blue Luminescence and Superstructures from Magic Size Clusters of CdSe. *Nano Lett.* **2009**, *9*, 514–518.
54. Winter, J. O.; Gomez, N.; Gatzert, S.; Schmidt, C. E.; Korgel, B. A. Variation of Cadmium Sulfide Nanoparticle Size and Photoluminescence Intensity with Altered Aqueous Synthesis Conditions. *Colloids Surf., A* **2005**, *254*, 147–157.
55. Murase, N.; Gaponik, N.; Weller, H. Effect of Chemical Composition on Luminescence of Thiol-Stabilized CdTe Nanocrystals. *Nanoscale Res. Lett.* **2007**, *2*, 230–234.
56. Liu, I. S.; Lo, H.-H.; Chien, C.-T.; Lin, Y.-Y.; Chen, C.-W.; Chen, Y.-F.; Su, W.-F.; Liou, S.-C. Enhancing Photoluminescence Quenching and Photoelectric Properties of CdSe Quantum Dots with Hole Accepting Ligands. *J. Mater. Chem.* **2008**, *18*, 675–682.
57. Pan, D. W. Q.; Jiang, S.; Ji, X.; An, L. Synthesis of Extremely Small CdSe and Highly Luminescent CdSe/CdS Core–Shell Nanocrystals *via* a Novel Two-Phase Thermal Approach. *Adv. Mater.* **2005**, *17*, 176–179.
58. Singha, A.; Satpati, B.; Satyam, P. V.; Roy, A. Electron and Phonon Confinement and Surface Phonon Modes in CdSe–CdS Core–Shell Nanocrystals. *J. Phys.: Condens. Matter* **2005**, *17*, 5697–5708.
59. Han, H.-Y.; Sheng, Z.-H.; Liang, J.-G. A Novel Method for the Preparation of Water-Soluble and Small-Size CdSe Quantum Dots. *Mater. Lett.* **2006**, *60*, 3782–3785.
60. Streckert, H. H.; Ellis, A. B. Mapping the Efficiency of Electron–Hole Pair Separation for a Semiconductor Electrode. Luminescent Properties of Graded Cadmium Sulfoselenide Electrodes. *J. Phys. Chem.* **1982**, *86*, 4921–4926.
61. Kim, D. I.; Islam, M. A.; Avila, L.; Herman, I. P. Contribution of the Loss of Nanocrystal Ligands to Interdot Coupling in Films of Small CdSe/1-Thioglycerol Nanocrystals. *J. Phys. Chem. B* **2003**, *107*, 6318–6323.

62. Socrates, G. *Infrared Characteristic Group Frequencies*; Wiley: New York, 1980.
63. Komada, S.; Kobayashi, T.; Arao, Y.; Tsuchiya, K.; Mori, Y. Optical Properties of Manganese-Doped Zinc Sulfide Nanoparticles Classified by Size Using Poor Solvent. *Adv. Powder Technol.* **2012**, *23*, 872–877.
64. Arora, A. K.; Rajalakshmi, M.; Ravindran, T. R.; Sivasubramanian, V. Raman Spectroscopy of Optical Phonon Confinement in Nanostructured Materials. *J. Raman Spectrosc.* **2007**, *38*, 604–617.
65. Campbell, I. H.; Fauchet, P. M. The Effects of Microcrystal Size and Shape on the One Phonon Raman-Spectra of Crystalline Semiconductors. *Solid State Commun.* **1986**, *58*, 739–741.
66. Lu, L.; Xu, X. L.; Liang, W. T.; Lu, H. F. Raman Analysis of CdSe/CdS Core−Shell Quantum Dots with Different CdS Shell Thickness. *J. Phys.: Condens. Matter* **2007**, *19*, 406221.
67. Richter, H.; Wang, Z. P.; Ley, L. The One Phonon Raman-Spectrum in Microcrystalline Silicon. *Solid State Commun.* **1981**, *39*, 625–629.
68. Comas, F.; Trallero-Giner, C. Interface Optical Phonons in Spherical Quantum-Dot/Quantum-Well Heterostructures. *Phys. Rev. B* **2003**, *67*, 115301.
69. Dzhagan, V. M.; Valakh, M. Y.; Raevska, O. E.; Stroyuk, O. L.; Kuchmiy, S. Y.; Zahn, D. R. T. The Influence of Shell Parameters on Phonons in Core−Shell Nanoparticles: A Resonant Raman Study. *Nanotechnology* **2009**, *20*, 365704.